



UNIVERSITÀ
DEGLI STUDI
FIRENZE

FLORE

Repository istituzionale dell'Università degli Studi di Firenze

Slow Relaxation of Magnetization in an Isostructural Series of Zinc-Lanthanide Complexes: An Integrated EPR and AC Susceptibility

Questa è la Versione finale referata (Post print/Accepted manuscript) della seguente pubblicazione:

Original Citation:

Slow Relaxation of Magnetization in an Isostructural Series of Zinc-Lanthanide Complexes: An Integrated EPR and AC Susceptibility Study / Amjad, Asma; Madalan, Augustin M; Andruh, Marius; Caneschi, Andrea; Sorace, Lorenzo. - In: CHEMISTRY-A EUROPEAN JOURNAL. - ISSN 0947-6539. - ELETTRONICO. - 22:(2016), pp. 12849-12858. [10.1002/chem.201601996]

Availability:

The webpage <https://hdl.handle.net/2158/1056498> of the repository was last updated on 2021-03-25T18:04:02Z

Published version:

DOI: 10.1002/chem.201601996

Terms of use:

Open Access

La pubblicazione è resa disponibile sotto le norme e i termini della licenza di deposito, secondo quanto stabilito dalla Policy per l'accesso aperto dell'Università degli Studi di Firenze (<https://www.sba.unifi.it/upload/policy-oa-2016-1.pdf>)

Publisher copyright claim:

La data sopra indicata si riferisce all'ultimo aggiornamento della scheda del Repository FloRe - The above-mentioned date refers to the last update of the record in the Institutional Repository FloRe

(Article begins on next page)

Slow relaxation of magnetization in an Isostructural series of Zinc-lanthanide complexes: an integrated EPR and AC susceptibility study

Asma Amjad^[a], Augustin M. Madalan^{*[b]}, Marius Andruh^[b], Andrea Caneschi^[a] & Lorenzo Sorace^{*[a]}

Dedication ((optional))

Abstract: We report the synthesis, structure, spectroscopic and dynamic magnetic properties of a series of heterodinuclear complexes, $[\text{ZnLn}(\text{LH}_4)_2](\text{NO}_3)_3 \cdot 6\text{H}_2\text{O}$ ($\text{Ln} = \text{Nd}, \text{Tb}, \text{Dy}, \text{Ho}, \text{Er}$ and Yb), with a new compartmentalized Schiff base ligand. The Ln^{III} ions in these systems show a distorted square antiprism geometry with a LnO_8 coordination sphere. EPR spectroscopy and dc magnetic studies show that the anisotropic nature of the complexes is far more complex than predicted on the basis of simple electrostatic model. Among the investigated systems only the Dy^{III} derivative showed single ion magnet behaviour, in zero and applied magnetic field, both in the pure polycrystalline samples and in a series of polycrystalline samples with different degrees of dilution at the single crystal level in the isostructural Y^{III} derivative. The rich dynamics observed as a function of frequency, field and temperature reveals that multiple relaxation mechanism are at play, resulting in a barrier of 189 cm^{-1} which is among the highest reported for dinuclear Zn-Dy systems. The analysis of the dynamic behaviour as a function of dilution degree further evidenced the survival of non-negligible intermolecular interactions even at the lowest dilution of 1%.

Introduction

The field of molecular magnetism has flourished over the last few decades owing to the fact that it allows access to understanding the fundamentals of quantum mechanical concepts, as well as providing real systems which are potential candidates for application purposes like molecular spintronics, hardware for quantum computing and high-density information storage.^[1-9] Currently, extensive interdisciplinary research is being conducted with lanthanides as the magnetic core for these molecular complexes:^[10] such systems quite often provide both large easy-axis magnetic anisotropy and high magnetic moment which are in principle necessary to observe magnetic bistability of molecular origin. The latter behavior is indeed usually attributed to the existence of an energy barrier, which at low temperatures hampers the reversal of magnetization. If no other relaxation

process is active the magnetization slowly relaxes following an Orbach process, and the thermal dependence of the relaxation rate follows an Arrhenius-like behavior. More importantly, at low enough temperature, the field dependent magnetization cycle show hysteresis, thus resulting in magnetic bistability of molecular origin. It is evident that in view of potential applications as molecular magnetic memories it is of utmost interest to maximize the temperature at which this behavior is observed, and this obviously requires the implementation of suitable strategies to increase the magnitude of anisotropy barrier (Δ).^[11] For lanthanides, the magnetic anisotropy is very sensitive to the geometry of the ligand field experienced by the lanthanide center. A simple electrostatic model is often used,^[12] to predict the anisotropy type on the basis of ligand field geometry which minimizes the repulsive interactions between the ligands and f-electron charge clouds. Those ions for which the electron density corresponding to largest M_J states has an oblate shape will show easy axis anisotropy when the largest electron densities from the ligands are located above and below the equatorial plane. The reverse will stand for a prolate electron-density shape. More appropriately, Rennes' group showed recently that atomic dipole moments (and not atomic charges) can be in some cases the driving force for the observed magnetic behaviour.^[13]

In addition to this "geometrical" approach for the obtainment of high anisotropy barriers, extremely interesting results have come forward from synthesis of magnetic core using compartmentalized Schiff base ligands which allows to combine 3d diamagnetic ions (such as Zn^{II}) with the lanthanides as core, to achieve higher anisotropy barriers (and hence higher blocking temperatures), than the corresponding complexes with the same ligand featuring only 4f ions.^[14] This phenomenon has been tentatively attributed both to a "dilution effect" brought about by the diamagnetic Zn^{II} ion and to an increase in electron density on the oxygen donor atoms that connect the Zn^{II} and Dy^{III} ions, provoked by coordination to Zn^{II} .^[15] However, structural effects induced by the Zn^{II} on the coordination sphere of the Dy^{III} ion can not be ruled out at this stage. Typical examples of ligands designed for synthesis of 3d-4f heteronuclear complexes are side-off bi-compartmental ligands derived from 2-hydroxy-3-methoxybenzaldehyde (*o*-vanillin) by condensation with various diamine (Scheme 1a). The 3d divalent metal ion organizes these podands in bi-compartmental ligands preparing the larger external $\text{O}_2\text{O}'_2$ compartment for lanthanide coordination. Depending on the ligand: 3d metal ion: lanthanide stoichiometry, 3d-4f heterobinuclear,^[16] or 3d-4f-3d heterotrinuclear units can be obtained.^[17]

More recently, several studies pointed out that relaxation of the magnetization can actually occur following different processes,^[18] characterized by different temperature and field dependences, as well as being influenced by the degree of

[a] Dr. A. Amjad, Prof. Dr. A. Caneschi, Prof. Dr. L. Sorace
INSTM Research Unit -LAMM, Dipartimento di Chimica "U-Schiff"
Università di Firenze
via della Lastruccia, 3-13, Sesto Fiorentino (FI), 50019, Italy.
E-mail: lorenzo.sorace@unifi.it

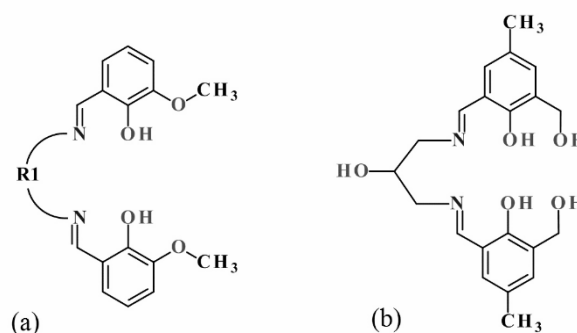
[b] Dr. A. M. Madalan, Prof. Dr. M. Andruh
Inorganic Chemistry Laboratory, Faculty of Chemistry
University of Bucharest, Str. Dumbrava Rosie nr. 23
020464-Bucharest, Romania.
E-mail: augustin.madalan@chimie.unibuc.ro

Supporting information for this article is given via a link at the end of the document.((Please delete this text if not appropriate))

intermolecular interactions. For example, quantum tunneling of magnetization (QTM) can be strongly effective in accelerating the relaxation in zero or low applied magnetic field even in Kramers systems, if dipolar interactions are not adequately suppressed. Further, on applying a magnetic field the direct relaxation process, occurring within the ground doublet, can become the dominant contribution due to the increasing number of available phonons of correct energy.^[19] Finally, deviations from simple Orbach-type relaxation may be due to Raman process which involves absorption of phonons promoting transitions to virtual energy states.^[20] It is becoming then increasingly evident that the simple observation of slow relaxation of magnetization is not necessarily connected to a process following Orbach relaxation process, and thus to the presence of a magnetic anisotropy barrier. In this respect, the simple electrostatic approach proposed above may not be always correct, and has to be thoroughly tested either experimentally or theoretically. While *ab initio* methods are often used for such purposes,^[20] these are still quite expensive in term of computing resources. In this respect, for Kramers' ions, a simple spectroscopic technique such as Electron Paramagnetic Resonance (EPR) may easily provide information about the type of anisotropy of the ground doublet, and in more fortunate case about its composition in term of $|M_J\rangle$ contributions. This allows testing the applicability of the electrostatic model, since in principle isostructural complexes containing lanthanides characterized by different shape (oblate or prolate) of the charge density for highest M_J should behave differently. More importantly, the observed anisotropy and composition of the ground doublet may be related to the observed magnetization dynamics, once this can be safely attributed to a single molecular process. It is worth noting in this framework that intermolecular interactions are often assumed to have negligible effects on the magnetization dynamics even at quite a high level ($> 10\%$) of paramagnetic ion concentration. To the best of our knowledge, only a few studies exist,^[20, 22-23] reporting the effect of systematic variation of paramagnetic ion concentration on the magnetization dynamics, while this is a crucial point to be assessed if single molecule properties have to be determined.

In this paper we report the synthesis, structure, EPR and dynamic magnetic properties of a series of heterodinuclear complexes, $[\text{ZnLn}(\text{LH}_4)_2](\text{NO}_3)_3 \cdot 6\text{H}_2\text{O}$ (hereafter **ZnLn**), containing a side-off bi-compartmental ligand obtained by reaction of 2-formyl-6-hydroxymethyl-*p*-cresol with 1,3-diamino-2-propanol (Scheme 1b). Because this ligand (LH_5) can generate two compartments very similar in size, the selection of the metal ions for each compartment is presumably driven by the oxophilicity of the lanthanides. Since our motivation was to investigate the magnetic behavior of lanthanide ions in the environment created by two such ligands, we chose to use the diamagnetic Zn^{II} , which plays only a structural role and may result, as previously outlined, in relatively large effective barrier to magnetization relaxation. The additional methyl groups on the phenyl rings of the ligand should minimize or prevent the intermolecular interactions between the metal ions. Insight into the anisotropy of the ground states of Kramers' ions and their composition was obtained using isothermal magnetization curves and EPR spectroscopy at X-band. The dynamic magnetic

properties of the whole series were investigated, the **ZnDy** derivative showing single molecule magnet (SMM) signatures. The analysis of its dynamics encompassed 5 frequency decades (10^{-1} – 10^4 Hz) and was conducted both on the pure derivative and on a series of differently diluted samples, hereafter identified as **ZnDy_aY_{1-a}** ($a = 0.01, 0.05, 0.25$) in zero and applied magnetic field. This revealed the persistence of relevant intermolecular interactions down to low Dy concentration and extremely rich low temperature spin dynamics.



Scheme 1. (a) Bi-compartmental ligands derived from *o*-vanillin by condensation with various diamine (b) and from 2-formyl-6-hydroxymethyl-*p*-cresol with 1,3-diamino-2-propanol.

Results and Discussion

Synthesis

The ability of the compartmental ligand derived from 2-formyl-6-hydroxymethyl-*p*-cresol and 1,3-diaminopropan to generate 3d-4f heterometal complexes was already proved.^[19] In a 1:1:1 stoichiometry between the 3d, 4f metal ions and the ligand, the 3d metal ion is located in the plane of the ligand while the 4f ion is out of the plane with a face exposed for coordination of auxiliary ligands. In our case, the reactions of the ligand LH_5 , the Schiff base obtained by condensation of 2-formyl-6-hydroxymethyl-*p*-cresol with 1,3-diamino-2-propanol (Scheme 1b), with zinc nitrate and lanthanide or yttrium nitrate in the molar ratio 2:1:1 afforded dinuclear compounds with general formula $[\text{ZnLn}(\text{LH}_4)_2](\text{NO}_3)_3 \cdot 6\text{H}_2\text{O}$. Temperature dependent $\chi_m T$ values of all the complexes (Figure S1 a-f), conformed to expectations, providing confirmation of the stoichiometry of the obtained complexes. Details on the synthesis and on chemical characterization can be found in the Experimental Section (see below), and further details can be found in the Supplementary Information.

X-ray structure determination

All the compounds of the series were found to crystallize in the space group $I4_1/a$, with isomorphic unit cell (see Table 1). In the following we will discuss, as an example for all the other systems, the structure of **ZnDy** derivative. The compound is made up of a tricationic $[\text{ZnDy}]^{3+}$ complex and three disordered nitrate anions, and contains six crystallization water molecules. However, the

disorder model of the nitrate anions and water molecules is not the same in all the crystals measured. The asymmetric unit is half of the molecule, which crystallize on a 4-fold rotoinversion axis (2-fold symmetry axis), made up by half Dy atom, half Zn atom and one ligand. Each ligand is mono-negative, since the two phenolic groups are deprotonated whereas one of the imino-groups is protonated, and folds as to coordinate through six atoms, one of them acting as bridge (Figure 1a).

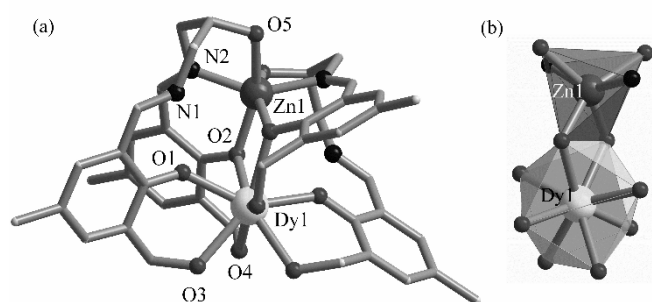


Figure 1. Perspective view of the dinuclear complex $[\text{ZnDy}(\text{LH}_4)_2]^{3+}$ in the crystal structure of the compound $[\text{ZnDy}(\text{LH}_4)_2](\text{NO}_3)_3 \cdot 6\text{H}_2\text{O}$ (a) and schematic representation of the coordination polyhedra for the two metal ions (b). The hydrogen atoms were omitted for clarity.

The Dy^{III} and Zn^{II} ions are bridged by two phenoxo oxygen atoms (one from each ligand) and the coordination sphere of the lanthanide ion is completed by two other phenoxo oxygens and the four benzylic oxygens, which remain protonated. The Dy–O bond lengths are: Dy1–O1 = 2.270(3), Dy1–O2 = 2.357(3), Dy1–O3 = 2.399(3) and Dy1–O4 = 2.399(4) Å. On the other hand, the Zn^{II} ion is hexa-coordinated with a distorted octahedron ZnO_4N_2 coordination geometry, the two nitrogens being the non-protonated imino- functions of the ligand, with bond length Zn1–N2 = 2.042(4) Å. In the coordination sphere of the Zn^{II} ion are also involved the oxygen atoms derived from 1,3-diamino-2-propanol, with bond length Zn1–O5 = 2.298(3) Å. The coordination geometry of the central Ln^{III} ion, in a LnO_8 environment, is very close to a square antiprism (Figure 1b), as obtained by continuous shape measurement analysis performed using Shape,^[24] ($S = 0.619$ compared to $S = 1.803$ for a triangular dodecahedron). The two faces of the idealized square antiprism are related by the two-fold symmetry axis passing through the Ln–Zn direction: the skew angle φ between the diagonals of the two square faces,^[25,10] is 42.37° compared to the ideal 45° angle; further, the two faces, which should be parallel in an ideal system, are actually making an angle of 5.6° . Due to this distortion, it is not possible to identify the resulting square antiprism as either elongated or compressed, since the angle between the idealized C_4 axis and the Ln–O directions is either larger or smaller than the magic angle depending on the O atom involved. On the other hand, the pseudo fourfold symmetry axis is almost perpendicular to the C_2 symmetry axis passing through the lanthanide and Zn^{II} ions ($\theta = 90.02^\circ$). The packing of the molecules in the lattice is such that the closest Dy–Dy intermolecular distance is 11.44 Å, with no direct hydrogen interactions or π – π stacking interactions involving adjacent ZnDy units.

For the doped samples, $[\text{ZnDy}_a\text{Y}_{1-a}(\text{LH}_4)_2](\text{NO}_3)_3 \cdot 6\text{H}_2\text{O}$, we measured by X-ray diffraction on single crystals three different crystals from the sample **ZnDy_{0.25}Y_{0.75}** and one from the sample **ZnDy_{0.05}Y_{0.95}** in order to check if the isomorphous dinuclear units $[\text{ZnDy}(\text{LH}_4)_2]^{3+}$ and $[\text{ZnY}(\text{LH}_4)_2]^{3+}$ are mixed in the lattice of the crystals (Table S1). In case of the three crystals from the sample **ZnDy_{0.25}Y_{0.75}** the best refinement parameters were obtained for the ratios Y:Dy = 0.76:0.24 (crystals **ZnDy_{0.25}Y_{0.75}-a** and **ZnDy_{0.25}Y_{0.75}-b**) and Y:Dy = 0.75:0.25 (crystal **ZnDy_{0.25}Y_{0.75}-c**). In the crystal **ZnDy_{0.05}Y_{0.95}** the ratio could not be reliably determined from the refinement: indeed, the same refinement parameters were obtained for ratios Y:Dy between 0.99:0.01 and 0.97:0.03.

Table 1. Crystallographic data, details of data collection and structure refinement parameters for compounds **ZnDy**, **ZnTb**, **ZnHo** and **ZnEr**.

Compound	ZnDy	ZnTb	ZnHo	ZnEr
Chemical formula	$\text{C}_{42}\text{H}_{62}\text{DyN}_7\text{O}_{25}$ Zn	$\text{C}_{42}\text{H}_{62}\text{TbN}_7\text{O}_{25}$ Zn	$\text{C}_{42}\text{H}_{62}\text{HoN}_7\text{O}_{25}$ Zn	$\text{C}_{42}\text{H}_{62}\text{ErN}_7\text{O}_{25}$ Zn
M (g mol ^{−1})	1292.85	1289.27	1295.28	1297.61
T (K)	200(2)	120(2)	293(2)	173(2)
λ (Å)	0.71073	0.71073	0.71073	0.71073
Crystal system	<i>Tetragonal</i>	<i>Tetragonal</i>	<i>Tetragonal</i>	<i>Tetragonal</i>
Space group	<i>I</i> 4 ₁ / <i>a</i>	<i>I</i> 4 ₁ / <i>a</i>	<i>I</i> 4 ₁ / <i>a</i>	<i>I</i> 4 ₁ / <i>a</i>
$a = b$ (Å)	16.1823(4)	16.1263(3)	16.2755(2)	16.183(2)
c (Å)	39.5572(12)	39.3631(11)	39.7057(8)	39.640(8)
V (Å ³)	10358.7(6)	10236.7(5)	10517.7(3)	10381(4)
Z	8	8	8	8
D_c (g cm ^{−3})	1.658	1.673	1.636	1.661
μ (mm ^{−1})	1.987	1.933	2.041	2.160
$F(000)$	5272	5264	5280	5288
Goodness-of-fit on F^2	0.989	1.072	1.124	0.872
$R1$ [$I > 2\sigma(I)$]	0.0412	0.0555	0.0449	0.0481
$wR2$ [$I > 2\sigma(I)$]	0.1235	0.1377	0.1169	0.1115
$R1$ (all)	0.0637	0.0818	0.0824	0.1122
$wR2$ (all)	0.1350	0.1650	0.1447	0.1375
Largest diff. peak and hole (eÅ ^{−3})	1.526, −1.012	2.551, −1.582	2.781, −1.231	0.832, −0.921

Ground state characterization

EPR spectroscopy is a powerful tool that allows an insight into the magnetic anisotropy of Ln-based complexes. Despite its historic importance in the understanding of electronic structure of Lanthanide based systems,^[26] its application to Ln-based molecular magnets gained impetus only recently.^[19a, 27] Among the investigated complexes of the present series, those characterized by an integer value of the J ground multiplet of the Ln^{III} ion (so-called non-Kramers ions: Ho^{III} and Tb^{III}) either did not show any EPR spectrum or the spectrum could not be analyzed

in term of an effective spin Hamiltonian.^[26] On the other hand, at 4 K the Kramers' ions Nd^{III} , Er^{III} and Yb^{III} revealed anisotropic spectra as shown in Figure 2. The EPR spectra were interpreted in terms of the spin Hamiltonian for a manifold ground state with effective spin $S_{\text{eff}} = 1/2$. Those of **ZnNd** and **ZnYb** clearly show an easy-axis type anisotropy of the ground state, i.e. $g_z > g_{xy}$, whereas for the **ZnEr** derivative $g_{xy} > g_z$ is observed, i.e. easy-plane anisotropy. For the case of **ZnYb** the set of peaks observed below 2 kOe, are due to parallel transitions of different Yb isotopes. The main peak at 1.65 kOe is attributed to the even isotopes of Yb ($I = 0$, global natural abundance 69.46%) and the two weaker ones to ^{171}Yb ($I = 1/2$, natural abundance 14.28%). The signal belonging to ^{173}Yb isotope ($I = 5/2$, natural abundance 16.13 %) is not observed probably because the corresponding structure is covered by the more intense transitions of the other isotopes.^[27a] The non-observation of an EPR spectrum for **ZnDy** derivative can be accounted for either by assuming a strong easy axis type anisotropy, resulting in a composition of the ground doublet which does not provide sufficient transition probability for a spectrum to be observed, or by considering that fast spin-lattice relaxation results in lines too broad to be observed.^[21f] Following this interpretation, simulations of the EPR spectra,^[28] were conducted on the basis of the following effective spin hamiltonian, where the hyperfine coupling term has been considered only for **ZnYb**:

$$\hat{H} = \beta S_{\text{eff}} \cdot g_{\text{eff}} \cdot H + \sum I \cdot A_{\text{eff}} \cdot S \quad (1)$$

Best simulations were obtained using the following parameters: **ZnNd**: $g_x = g_y = 2.15$, $g_z = 4.35$; **ZnEr**: $g_x = g_y = 7.2$, $g_z = 1.95$; **ZnYb**: $g_x = g_y = 1.79$, $g_z = 6.19$ ($A_x = A_y = 0.023 \text{ cm}^{-1}$, $A_z = 0.043 \text{ cm}^{-1}$) as shown in Figure 2.

Complementary information on the properties of the lowest lying levels different derivatives of the series could be obtained by measuring the isothermal magnetization M as a function of applied magnetic field H (Figure S1 (g-l)) up to 50 kOe. While **ZnHo** and **ZnDy** show magnetization saturated at $5.18 \mu_B$ and $5.36 \mu_B$ respectively even at 4.5 K, for **ZnNd**, **ZnEr** and **ZnYb** complexes even at the lowest measured temperature complete saturation is not achieved. In particular, for **ZnEr** derivative, the magnetization follows a linear trend at high field, even if the magnetizations measured at the two temperatures are coincident. This behaviour suggests the presence of a close lying state which results in a sizable Van Vleck paramagnetic contribution. Accordingly, for this derivative the simulation of the M vs H curves using EPR derived parameters does not provide a reasonable fit. On the contrary, the observation of saturation for **ZnHo** and **ZnDy** complexes points to a well isolated ground doublet (or pseudo-triplet for **ZnHo**) and the non-superimposability of the M vs H curves confirms their magnetic anisotropy. Finally, the M vs H curves for **ZnNd** and **ZnYb** were nicely fit using PHI,^[29] based on Hamiltonian (1) without considering hyperfine coupling and provided parameters in good agreement with EPR ones; **ZnYb**: $g_{xy} = 1.99$, $g_z = 6.54$, **ZnNd**: $g_{xy} = 2.46$, $g_z = 4.12$.

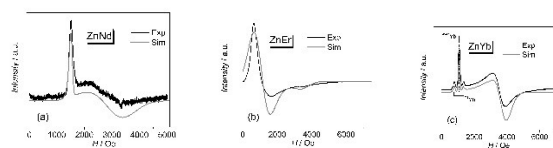


Figure 2. X-band EPR spectra of microcrystalline powder samples of the **ZnLn** family, measured at 5 K. (a): Ln = Nd; (b) Ln=Er; (c) Ln=Yb. Grey lines are the simulated spectra using parameters reported in the text.

The parameters of the effective Spin Hamiltonian obtained for the Kramers derivatives of the series deserve some comments. Following the approach popularized by Long and Rinehart,^[12b] an axially elongated coordination geometry around the lanthanide ion, such as the one observed in our case, should favor the stabilization of a ground doublet with large M_J for oblate type ions (Ce, Pr, Nd, Tb, Dy, Ho). This would provide easy axis type anisotropy for these ions, while easy plane anisotropy should be observed for the remaining ions. However, both EPR spectroscopy and M vs H curves indicate that this is not the case in this series; indeed, **ZnYb** and **ZnNd** show easy axis type anisotropy, whereas **ZnEr** is easy-plane. This apparent inconsistency may be attributed to the oversimplified view of the analysis of the effect of the ligand as being only electrostatic and in a purely axial environment. Indeed, the deviation from purely axial symmetry of the ligand field is witnessed by the observation of relatively large g_{xy} components also for easy axis type complexes. This indicates that different M_J 's contributes to the ground doublet (and to each doublet, actually). In particular, the analysis of the EPR spectrum of **ZnYb** allows to appreciate the effect of distortion from tetragonal symmetry. Indeed, in the assumption of idealized geometry, the contributing M_J will be related by $M_J' = M_J \pm 4$ meaning that each doublet can only be described by one of the two following linear combinations:^[27(a), 30]

$$\cos\theta \left| \pm \frac{7}{2} \right\rangle + \sin\theta \left| \mp \frac{1}{2} \right\rangle \quad (2a)$$

$$\cos\theta \left| \pm \frac{5}{2} \right\rangle + \sin\theta \left| \mp \frac{3}{2} \right\rangle \quad (2b)$$

It is however readily seen that it is not possible, by assuming such a simple scheme, to reproduce the experimentally observed g values. At any rate, the observed g_z for **ZnYb** points to a major contribution of the $|\pm 7/2\rangle$ M_J state (expected $g_z = 8$, $g_{xy} = 0$). In much the same way, the observed g values indicate that the ground doublet of Er^{III} in **ZnEr** has major contribution from $M_J = |\pm 1/2\rangle$ (expected $g_{xy} = 9.6$, $g_z = 1.2$), whereas Nd^{III} in **ZnNd** is more isotropic.

Magnetization Dynamics

To inspect magnetization relaxation processes in the family under study, ac susceptibility measurements were performed as a function of external applied field (0 -1.2 kOe) temperature (2-30 K) and frequencies (0.1 Hz - 10 kHz). In the case of **ZnHo** and **ZnEr** compounds a clear maximum was observed around 5 K in the in-phase ac signal χ' as a function of temperature (Figure S2),

with no frequency dependence. This behavior suggests weak intermolecular antiferromagnetic interactions are active in both these complexes, despite the large intermolecular distance among the complexes of the series. On the other hand, only **ZnDy** showed frequency dependent out of phase signal (χ''_m), both in zero and applied field, suggestive of SMM behavior. Figure 3 (Left) shows the field dependence of the out-of-phase ac susceptibility χ''_m of the **ZnDy** complex observed at 2 K: a clear maximum (peak 1) is observed at zero field around 40 Hz, the magnitude of which decreased as soon as the field was increased to 100 Oe, disappearing for field larger than 400 Oe. Simultaneously a second peak appears at lower frequencies ($\nu < 1$ Hz), which increases in intensity and moves to lower frequency on increasing the field. Based on the field dependent behavior, an extensive temperature study (2 to 30 K) was conducted at both zero and 1 kOe external applied field. It is evident that while only a weak temperature dependence of the χ''_m signal is observed for the high frequency process occurring in zero field, a more pronounced dependence is observed in the presence of dc external field for the low frequency process (Figure S3 and Figure 3a/b).^[31] As a whole, the observed behaviour is strongly reminiscent of the one first observed in $[\text{Dy}(\text{DOTA})(\text{H}_2\text{O})]^-$ derivatives by Sessoli and coworkers.^[32]

In order to clarify the observed phenomena, ac susceptibility data were fit using a generalized Debye equation to extract the relaxation times at different temperature and fields. The results are shown as Arrhenius plot in Figure 3d. For the zero field data, two regimes are clearly identified; a low temperature region ($T < 10$ K), where the relaxation rate is essentially temperature independent, suggesting a pure quantum tunneling regime; and a higher temperature one ($T > 15$ K), where the rate rapidly increases suggesting the dominance of thermal relaxation. This can occur either via two-phonon Orbach process or via Raman process. In the presence of an external field of 1 kOe the relaxation time is significantly increased in the low temperature regime ($T < 10$ K). This behavior agrees well with the fact that the application of a dc field is expected to suppress the quantum tunneling of magnetization, making thermally activated mechanisms dominant. In agreement with this interpretation, no significant change is observed upon field application in the thermally activated regime. It is further to be noted that the significant deviation from linear behavior in the intermediate temperature region, even on applying a field, suggests the concomitant effectiveness of different thermally activated processes.

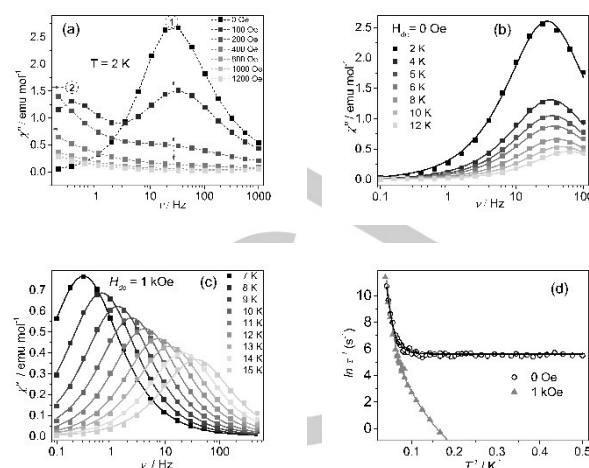


Figure 3. (a) Field dependence of out-of-phase χ''_m ac susceptibility of **ZnDy** complex, observed at 2 K. The dotted arrows indicate the two different relaxation processes observed in this system. Dashed lines are guide to the eye (b) Frequency dependence of out-of-phase ac susceptibility and corresponding Debye fits of **ZnDy** complex at 0 Oe and variable temperatures c) Frequency dependence of out-of-phase ac susceptibility of **ZnDy** complex and corresponding Debye fits at 1 kOe and variable temperatures d) Arrhenius plot of the temperature dependence of the relaxation rate of **ZnDy**, with and without an applied field.

The observed behavior was then quantitatively analyzed taking into account all the mentioned processes;

$$\tau^{-1} = \tau_{QTM}^{-1} + \tau_0^{-1} \exp\left(-\frac{\Delta}{k_B T}\right) + C T^n \quad (3)$$

where the first term represents the quantum tunneling process, the second term is the Orbach process, and the last term is the Raman process. The direct term, which should in principle be present for the 1 kOe dataset was not explicitly considered to avoid overparametrization: on the other hand, the extremely slow dynamics at lower temperature does not allow to estimate it from the field dependence of the relaxation rate as elsewhere reported.^[18a, 32] The data fitting was addressed by including contributions of each process step by step. In particular, the linear shape of the Arrhenius plot at high temperatures suggested that the Orbach process is dominant at $T > 17$ K allowing a reliable estimate of this term. The corresponding fit in this region provides as best fit parameters $\Delta = 189$ cm⁻¹ and $\tau_0 = 2.67 \times 10^{-10}$ s, conveniently falling in the range expected for lanthanide-based SMMs.^[26] The other parameters obtained from fits of both in-field and zero field are reported in Table 2. The effective bistability, which is a hallmark of single molecule magnet behavior, was confirmed for **ZnDy** by magnetization versus field measurements at 2 K (Figure 4a). A clear butterfly hysteresis is observed, in agreement with relatively fast zero-field relaxation and slow relaxation in external applied field. Analysis of the dM/dH curve clearly shows that the tunneling is actually occurring at ± 300 Oe (Figure S4), due to the internal dipolar fields.^[33]

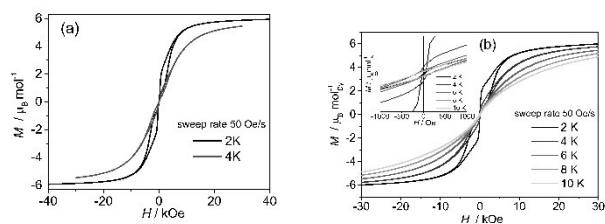


Figure 4: (a) Hysteresis curves of **ZnDy** complex at 2 K and 4 K (b) Hysteresis curves of **ZnDy_{0.01}Y_{0.99}** complex at temperatures between 2 and 10 K. The inset shows a close-up view of the zero field region, evidencing the non zero coercive field even for relatively high temperatures. Magnetization values for doped sample are rescaled per mole of Dy ions.

Magnetization dynamics of **ZnDy_aY_{1-a}**

In order to probe the role of inter-molecular dipolar interactions on the observed magnetic properties of the **ZnDy** complex, i.e. if the slow relaxation of magnetization observed for this complex is an intrinsic molecular property, diluted samples **ZnDy_aY_{1-a}** ($a = 0.01, 0.05, 0.25$) containing **ZnDy** diluted in a diamagnetic isostructural host lattice of yttrium (**ZnY**) were obtained and characterized. The crystal structures of these samples were verified and all diluted samples were found to be iso-structural (Table 2, Figure S4 and Table S2) with the pure **ZnDy** and **ZnY** derivative (i.e. the substitution of the $[\text{YZn}(\text{LH}_4)_2]^{3+}$ cations with $[\text{DyZn}(\text{LH}_4)_2]^{3+}$ ones takes place statistically in the crystal lattice). This is also confirmed by the magnitude of normalized M vs H curves showing the same behaviour as the pure compound (Figure S5). The concentration of Dy^{III} in the diluted phase was estimated from the factor necessary to rescale the isothermal magnetization curves at low temperature onto the corresponding curves of the pure phase, providing doping concentration close to the one calculated on the basis of the stoichiometry (Table S3). All the doped samples show slow relaxation of the magnetization, both in zero and applied field: the observed dynamics as a function of field and temperature are shown in Figures S6–S8. It is evident that in the low temperature region ($T < 4$ K) the relaxation times increase, as expected, with dilution. Further, as already observed for the pure sample, application of a static field results in a slowing down of the relaxation, even for the most diluted samples (Figure 5, right).

For a quantitative analysis of these data the relaxation times of the three doped samples and of the pure one were extracted from the Debye fits of the χ''_m curves (Figure S6–S8) measured with and without field, and are shown in the $\ln \tau^{-1}$ vs T^{-1} plot in Figure 5. A more conventional plot of $\ln \tau$ vs T^{-1} is shown in Figure S9 for convenience. In the low temperature region, the decrease in Dy^{III} content results not only in an increase of the relaxation time, but also in an increase of the temperature dependence below 5 K: this indicates that QTM is increasingly less efficient on increased doping. However, since the temperature dependences observed for $a = 0.05$ and $a = 0.01$ are not superimposable, it is possible to conclude that even at this low concentration, and despite the large intermolecular distance and the absence of any reliable intermolecular interaction path, the relaxation behavior is still influenced by intermolecular interactions, promoting quantum tunneling. On increasing temperature, the role of thermally activated process is obviously increasing, and the **ZnDy_{0.01}Y_{0.99}** and **ZnDy_{0.05}Y_{0.95}** relaxation curves superimpose above 5 K.

Finally, for $T > 10$ K the relaxation rates are the same for all the four investigated samples, indicating that relaxation is no more affected by intermolecular interactions but it is dominated by single molecule, thermally activated processes. According to this interpretation the observed results, both in-field and zero-field were tentatively analyzed using equation 3. The observed relaxation times in zero field as a function of temperature were fitted (solid lines in Figure 5 (a)) by keeping the Orbach term constant for all the 4 concentrations (according to its single molecular origin reflecting the presence of an excited state at a given energy^[18a,18d,34]) and having the Raman term varying along the series. It is worth noting that, consistently with the decrease in dipolar interactions upon dilution, a decrease in the quantum tunneling rate τ_{QTM}^{-1} with a decrease of Dy^{III} concentration is observed, whereas the obtained Raman exponents, despite being in the expected range,^[18c,35] have to be considered as phenomenological, not following a constant trend.

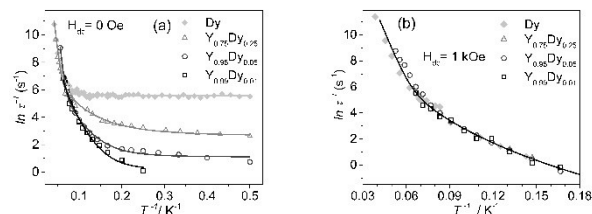


Figure 5. Temperature dependence of the relaxation times of the **ZnDy_aY_{1-a}** complex ($a = 1, 0.01, 0.05$ and 0.25) in 0 (a) and 1 kOe (b) applied dc magnetic field. Continuous lines are best fit obtained using parameters reported in Table 2.

Interestingly, no deviation in relaxation times of the doped samples from the concentrated one was observed in the presence of the applied field. As shown in Figure 5b, the temperature dependence of τ for all the four samples superimpose on a single curve: hence, one can deduce that the applied field is large enough to suppress any intermolecular interaction present in the system able to promote QTM, at any doping level. The corresponding curves are then described by the same parameters as those of the pure sample. Following the extremely slow relaxation time observed at low temperature, magnetic hysteresis measurements were performed on the **ZnDy_{0.01}Y_{0.99}** complex; remarkably even with a reasonably slow field scan rate of 50 Oe/s a partially open cycle was observed up to 10 K with a coercive field of about 260 Oe, which is larger than the experimental uncertainty (Figure 4 (b) and Figure S10). The hysteresis is clearly characterized by a dominant zero-field tunneling, witnessed by the large step in zero field which is particularly efficient in promoting the tunneling at low temperature, leading to a negligibly small coercive field at 2 K, while at higher temperature it is less effective. Analysis of the dM/dH curve further evidences the presence of an additional peak (Figure S11) at negative (positive) field when sweeping from positive (negative) magnetization. The field value at which this is observed is clearly decreasing on increasing temperature: this suggests that also in this case the origin of this process is in the intermolecular dipolar interactions.^[32] As a whole these results are of particular interest since – together with the observed temperature dependence of τ in zero field – they

underline that even for dilution down to 1% in a system in which the closest Dy-Dy distance in the pure sample is larger than 10 Å the dipolar effect can be non-negligible.^[36] The reason for such a behaviour should probably be traced back to the large number of close-contacts among Dy ions in the lattice, leading to average distances which are still too short, even in high dilution, to consider dipolar interaction negligible.

Table 2. Fitting parameters of the relaxation mechanisms for the differently doped complexes in zero applied field.

	ZnDy	ZnDy _{0.25} Y _{0.75}	ZnDy _{0.05} Y _{0.95}	ZnDy _{0.01} Y _{0.99}
<i>n</i>	6	2.88	4.5	6 ± 0.2
<i>C</i> / s ⁻¹ K ⁻ⁿ	(4±0.3)×10 ⁻⁵	0.15±0.01	(1.5±0.2) ×10 ⁻³	(4±1)×10 ⁻⁵
τ_{QTM}^{-1} / s ⁻¹	270±5	15±1	5±1	1.1±0.3
τ_0 / s	2.67 ×10 ⁻¹⁰	2.67×10 ⁻¹⁰	2.67×10 ⁻¹⁰	2.67×10 ⁻¹⁰
Δ / cm ⁻¹	189	189	189	189

Finally, we wish to discuss the observed energy barrier in comparison with the effective ones reported for other dinuclear Zn-Dy systems: those for which U_{eff} has been determined almost invariably show much lower values (see Table 3).^[15, 37] To the best of our knowledge only a single exception has been reported, namely the system described by Watanabe et al.^[38] containing a 9-coordinated Dy center. In that case the reason for such a high energy barrier was attributed to the presence of a strongly axial ligand field induced by the negative charge on phenolato oxygens of both Schiff base and salicylaldehyde ligands. More recently, as discussed in the introduction, Rajaraman and coworkers suggested that the increase in the barrier observed in Zn-Dy systems compared to complexes of the same ligand containing only Dy^{III}, can be related to the larger negative charge on the bridging phenolato oxygens induced by the neighboring Zn ion.^[15] Furthermore, an increase in the barrier was anticipated with increased symmetry of the system. In this respect the case treated here, for which Dy^{III} sits on a crystallographic C₂ symmetry axis, is particularly favorable, since this induces a perfect planarity of the DyO₂Zn core. More information on this point were obtained by performing test calculations based on the electrostatic model using Magellan,^[39] even if the obtained results should be considered with caution. Indeed, as discussed above, EPR spectroscopy on the whole series showed that a pure electrostatic model is not able to describe the variation of the properties along the series. Nonetheless, starting from the fractional charges on the donating atoms calculated in,^[15] an axial ground state with an energy barrier comparable to the experimental one can be obtained (see supplementary material for details). We stress that the calculated energy barrier turned out to be extremely sensitive to the fractional charge on the phenolic oxygens, for which variations of ± 0.1 around the assumed value of -0.6 and -0.7 (for the single bound and bridging one, respectively), result in values differing by a factor larger than two (Table S4). On the other hand, the calculated direction of the symmetry axis is not lying along the

binary axis but in the plane perpendicular to it (Figure S12), forming an angle of ca. 20° with the Dy-O1 direction, being quite insensitive to small variations of charge distribution. As a whole, the results of the calculations within the electrostatic model evidence that an axial ground state is likely to occur for **ZnDy**, thus explaining the absence of an EPR signal for this derivative, and that the anisotropy barrier obtained by magnetic characterization is consistent with expectations.

Table 3. Comparison of the effective anisotropy barriers reported in literature for dinuclear Zn-Dy systems.

Molecule (CSD Code)	U_{eff} / cm ⁻¹	Ref.	Dy coordination sphere
ZOFMEO	25.4	37 (a)	DyO8
DAYZEK	27.4	37 (b)	DyO10
TISZAY	28.5	37 (c)	DyO9
ROCXYO	83	15	DyO9
WOZZOC	36	37 (d)	DyO9
EWEPAY	229.3	38	DyO9
ZOFMEO	189	This work	DyO8

Conclusions

We reported here the synthesis, structural and magnetic characterization of a new isostructural series of **ZnLn** dinuclear systems obtained by using a newly designed compartmentalized Schiff base. The Ln^{III} ion in these systems shows a distorted square antiprism geometry with a LnO₈ coordination sphere. EPR spectra and isothermal magnetization measurements on Kramers ion derivatives evidenced a large distortion from an idealized axial structure, with ground state wave functions having contributions by many different M_J sublevels; the only possible exception being **ZnDy**, for which no EPR could be observed. In agreement with this interpretation, the only derivative showing slow relaxation of the magnetization in zero field turned out to be the **ZnDy** derivative, the dynamics of which has been investigated as a function of field, frequency, temperature and degree of dilution in the isostructural Y^{III} derivative. The results of the analysis unequivocally indicate that the system relaxes through a combination of processes (Raman, QTM and Orbach) with an anisotropy barrier which is one of the highest for this type of systems. This was attributed both to the larger negative charge induced on the bridging phenolato oxygen atoms by the presence of the neighbouring Zn^{II} cation and by the relatively high symmetry of the molecule, crystallographically imposed. The study also evidenced that to obtain reliably diluted systems in which the dipolar interactions are not affecting the relaxation in zero field, promoting tunneling, even a 1% degree of dilution might not be enough. This is of particular relevance for a meaningful analysis and comparison of relaxation properties of Ln-based SMM and of their real anisotropy barriers.

Experimental Section

Synthesis

All the chemicals used as well as all the solvents were purchased from commercial sources. The 2-formyl-6-hydroxymethyl-*p*-cresol was synthesized following reported experimental procedures.^[18] All the heterodinuclear complexes, $[\text{ZnLn}(\text{LH}_4)_2](\text{NO}_3)_3 \cdot 6\text{H}_2\text{O}$, were synthesized following the same general procedure. 1 mmol of 2-formyl-6-hydroxymethyl-*p*-cresol and 0.5 mmol of 1,3-diamino-2-propanol were stirred at room temperature for two hours in 50 mL of methanol. Subsequently were added 0.25 mmol of $\text{Zn}(\text{NO}_3)_2 \cdot 6\text{H}_2\text{O}$ and 0.25 mmol of $\text{Y}(\text{NO}_3)_3 \cdot 6\text{H}_2\text{O}$ or $\text{Ln}(\text{NO}_3)_3 \cdot x\text{H}_2\text{O}$ ($\text{Ln}^{\text{III}} = \text{Nd}^{\text{III}}, \text{Tb}^{\text{III}}, \text{Dy}^{\text{III}}, \text{Ho}^{\text{III}}, \text{Er}^{\text{III}}, \text{Yb}^{\text{III}}$) dissolved in 25 mL of water and stirred for three more hours. The reaction mixtures were left for slow evaporation at room temperature. In 5–10 days the yellow crystals of the dinuclear complexes, $[\text{ZnLn}(\text{LH}_4)_2](\text{NO}_3)_3 \cdot 6\text{H}_2\text{O}$, were formed. The crystals were collected by filtration prior total evaporation of the solvent to prevent contamination with side products. The yields range between 40 and 65 percent. The diluted $[\text{ZnDy}_x\text{Y}_{(1-x)}(\text{LH}_4)_2](\text{NO}_3)_3 \cdot 6\text{H}_2\text{O}$ samples were obtained dissolving in the minimum amount of mixture methanol-water (3:1) the complexes $[\text{ZnDy}(\text{LH}_4)_2](\text{NO}_3)_3 \cdot 6\text{H}_2\text{O}$ and $[\text{ZnY}(\text{LH}_4)_2](\text{NO}_3)_3 \cdot 6\text{H}_2\text{O}$ in the ratios: 0.25:0.75, 0.05:0.95 and 0.01:0.99, respectively. The yellow crystals of doped samples, $[\text{ZnDy}_x\text{Y}_{(1-x)}(\text{LH}_4)_2](\text{NO}_3)_3 \cdot 6\text{H}_2\text{O}$, grown in 1–3 days by slow evaporation of the solvent. Elemental analyses. $[\text{ZnY}(\text{LH}_4)_2](\text{NO}_3)_3 \cdot 6\text{H}_2\text{O}$, calculated: C 41.37%, H 5.13%, N 8.04%, found: C 41.20%, H 5.09%, N 7.90%. $[\text{ZnDy}(\text{LH}_4)_2](\text{NO}_3)_3 \cdot 6\text{H}_2\text{O}$, calculated: C 39.02%, H 4.83%, N 7.58%, found: C 38.99%, H 4.74%, N 7.48%. $[\text{ZnDy}_{0.25}\text{Y}_{0.75}(\text{LH}_4)_2](\text{NO}_3)_3 \cdot 6\text{H}_2\text{O}$, calculated: C 40.76%, H 5.05%, N 7.92%, found: C 40.59%, H 5.02%, N 7.83%. $[\text{ZnDy}_{0.05}\text{Y}_{0.95}(\text{LH}_4)_2](\text{NO}_3)_3 \cdot 6\text{H}_2\text{O}$, calculated: C 41.25%, H 5.11%, N 8.02%, found: C 41.16%, H 5.05%, N 7.90%. $[\text{ZnDy}_{0.01}\text{Y}_{0.99}(\text{LH}_4)_2](\text{NO}_3)_3 \cdot 6\text{H}_2\text{O}$, calculated: C 41.35%, H 5.12%, N 8.04%, found: C 41.22%, H 5.05%, N 7.92%. ICP data (Table S3) were obtained using a Optima 2000 DV OES Perkin Elmer spectrometer.

Magnetic characterisation

X-band ($\nu = 9.41$ GHz) spectroscopic studies on the microcrystalline powder samples were carried out at low temperatures using a E500 Bruker spectrometer equipped with a ESR900 (Oxford instruments) continuous flow ^4He cryostat. Temperature dependent direct current (dc) magnetic measurements were conducted on a Quantum Design MPMS SQUID magnetometer. Ac magnetic susceptibility measurements were carried out both on the aforementioned SQUID and on a Quantum Design PPMS in ac mode at both zero and applied external dc field in the presence of 5 Oe oscillating magnetic field. The latter setup was used for frequencies between 10 Hz and 10 KHz whereas the former one was used for frequencies in the range 0.1 Hz to 1 KHz. Hysteresis cycles at fixed temperature were measured using the VSM option of the Quantum Design PPMS. The purity of the microcrystalline powders used for magnetic and EPR characterization and their coincidence with the molecular structure determined by single crystal X-ray diffraction was preliminarily checked by X-ray powder diffraction. X-ray powder diffraction patterns of the pure samples were carried on a Bruker D8 advance powder diffractometer equipped with a Cu source ($K\alpha$, $\lambda = 1.54\text{\AA}$). The resulting spectra were found to be consistent with the ones expected on the basis of the molecular structure obtained by single crystal X-ray diffraction (Figure S13). Single crystal X-ray diffraction measurements were performed on STOE IPDS II and Xcalibur Sapphire3 diffractometers, both operating with Mo- $K\alpha$ ($\lambda = 0.71073$ Å) X-ray tube with graphite monochromators.

Crystallographic data collection and structure determination

Single crystal X-ray diffraction measurements were performed on a STOE IPDS II diffractometer for the compounds **ZnY**, **ZnDy**, **ZnDy_{0.25}Y_{0.75}-a/b/c** (**a**, **b** and **c** identifying three different measured single crystals of the same sample **ZnDy_{0.25}Y_{0.75}**), **ZnDy_{0.05}Y_{0.95}**, and **ZnEr**, and on a Xcalibur, Sapphire3 diffractometer for the compounds **ZnTb** and **ZnHo**, both operating with Mo- $K\alpha$ ($\lambda = 0.71073$ Å) X-ray tube with graphite monochromator. The structures were solved by direct methods and refined

by full-matrix least squares techniques based on F^2 . The non-H atoms were refined with anisotropic displacement parameters. Calculations were performed using SHELX-2013/2014 crystallographic software package. A summary of the crystallographic data and the structure refinement for crystals **ZnY**, **ZnDy**, **ZnDy_{0.25}Y_{0.75}-a/b/c**, **ZnDy_{0.05}Y_{0.95}**, **ZnEr**, **ZnTb** and **ZnHo** are given in Table 1 and Table S1. CCDC 1474018–1474026 contains the crystallographic information file for this paper. These data are provided free of charge by The Cambridge Crystallographic Data Centre (<http://ccdc.cam.ac.uk/>). Only the unit cells were determined for the compounds **ZnDy_{0.01}Y_{0.99}**, **ZnNd** and **ZnYb** (Table S2).

Acknowledgements

We acknowledge the financial support of Italian MIUR through the project Futuro in Ricerca 2012 (RBF12RPD1) and of the Italian and Romanian foreign affair secretariat through the project Multifunctional Molecular Nanosystems. AMM acknowledges also support from Romanian National Authority for Scientific Research, CNCS – UEFISCDI, project number PN-II-RU-TE-2011-3-0252.

Keywords: Lanthanide; Single Ion Magnets; EPR spectroscopy; Ac susceptibility; Zinc

- [1] O. Kahn, *Molecular Magnetism*, Wiley-VCH **1993**
- [2] D. Gatteschi, R. Sessoli and J. Villain in *Molecular Nanomagnets*, Oxford University Press, Oxford, **2006**.
- [3] L. Bogani, W. Wernsdorfer, *Nature Mater.* **2008**, *7*, 179–186
- [4] F. Troiani, M. Affronte *Chem. Soc. Rev.* **2011**, *40*, 3119–3129
- [5] J. R. Friedman and M. P. Sarachik, *Annu. Rev. Condens. Matter Phys.* **2010**, *1*, 109–128.
- [6] *Molecular Magnets Physics and Applications*, (Eds.: J. Bartolomé, F. Luis, J. F. Fernández), Springer, **2014**.
- [7] A. Dei, D. Gatteschi *Angew. Chem. Int. Ed.* **2011**, *50*, 11852–11858
- [8] O. Sato, J. Tao, Y. Z. Zhang, *Angew. Chem., Int. Ed.*, **2007**, *46*, 2152–2187
- [9] *Molecular Nanomagnets and related phenomena* (Ed: S. Gao) *Structure and Bonding* **2015**, *164*
- [10] a) L. Sorace, C. Benelli and D. Gatteschi, *Chem. Soc. Rev.* **2011**, *40*, 3092–3104; b) S. T. Liddle and J. van Slageren in *Lanthanides and Actinides in Molecular Magnetism*, (Eds.: R. Layfield, M. Murugesu), Wiley-VCH, Weinheim **2015**, pp. 315–336.
- [11] a) M. Gregson, N. F. Chilton, A. Ariciu, F. Tuna, I. F. Crowe, W. Lewis, A. J. Blake, D. Collison, E. J. L. McInnes, R. E. P. Winpenny and S. T. Liddle, *Chem. Sci.* **2016**, *7*, 155–165; b) J. Liu, Y. Chen, J. Liu, V. Vieru, L. Ungur, J. Jia, L. F. Chibotaru, Y. Lan, W. Wernsdorfer, S. Gao, X. Chen, M. Tong, *J. Am. Chem. Soc.* **2016**, *138*, 5441–5450; c) S. K. Gupta, T. Rajeshkumar, G. Rajaraman and R. Murugavel, *Chem. Sci.* **2016**, DOI: 10.1039/c6sc00279j.
- [12] a) J. Sievers, *Z. Phys. B: Condens. Matter Quanta*, **1982**, *45*, 289; b) J. D. Rinehart and J. R. Long, *Chem. Sci.* **2011**, *2*, 2078–2085.
- [13] J. Jung, X. Yi, G. Huang, G. Calvez, C. Daguebonne, O. Guillou, O. Cadot, A. Caneschi, T. Roisnel, B. Le Guennic and K. Bernot, *Dalton Trans.* **2015**, *44*, 18270–18275
- [14] a) D. N. Woodruff, R. E. P. Winpenny and R. A. Layfield, *Chem. Rev.* **2013**, *113* (7), 5110–5148; b) K. Liu, W. Shi and P. Cheng, *Coord. Chem. Rev.* **2015**, *289*, 74–122.
- [15] A. Upadhyay, S. K. Singh, C. Das, R. Mondol, S. K. Langley, K. S. Murray, G. Rajaraman and M. Shanmugam, *Chem. Commun.* **2014**, *50*, 8838–8841.
- [16] a) J.-P. Costes, F. Dahan, A. Dupuis and J.-P. Laurent, *Inorg. Chem.* **1996**, *35*, 2400–2402; b) J.-P. Costes, F. Dahan and A. Dupuis, *Inorg. Chem.* **1997**, *36*, 4284–4286; c) T. D. Pasatoiu, J.-P. Sutter, A. M. Madalan, F. Z. C. Fella, C. Duhayon and M. Andruh, *Inorg. Chem.* **2011**, *50*, 5890–5898; d) T. D. Pasatoiu, C. Tiseanu, A. M. Madalan, B. Jurca, C. Duhayon, J.-P. Sutter and M. Andruh, *Inorg. Chem.* **2011**, *50*, 5879–5889.

- [17] a) A. M. Madalan, N. Avarvari, M. Fourmigué, R. Clérac, L. F. Chibotaru, S. Clima and M. Andruh, *Inorg. Chem.* **2008**, *47*, 940-950; b) D. Visinescu, A. M. Madalan, M. Andruh, C. Duhayon, J.-P. Sutter, L. Ungur, W. van den Heuvel and L. F. Chibotaru, *Chem. Eur. J.* **2009**, *15*, 11808-11814; c) J.-P. Costes, S. Titos-Padilla, I. Oyarzabal, T. Gupta, C. Duhayon, G. Rajaraman, and E. Colacio, *Chem. Eur. J.* **2015**, *21*, 15785-15796; d) S. Das, K. S. Bejoymohandas, A. Dey, S. Biswas, M. L. P. Reddy, R. Morales, E. Ruiz, S. Titos-Padilla, E. Colacio, and V. Chandrasekhar, *Chem. Eur. J.* **2015**, *21*, 6449-6464.
- [18] a) E. Lucaccini, L. Sorace, M. Perfetti, J.-P. Costes, R. Sessoli, *Chem. Commun.* **2014**, *50*, 1648-1651; b) R. J. Blagg, L. Ungur, F. Tuna, J. Speak, P. Comar, D. Collison, W. Wernsdorfer, E. J. McInnes, L. F. Chibotaru, R. E. Winpenny, *Nature Chem.* **2013**, *5*, 673-678; c) J.-L. Liu, K. Yuan, J.-D. Leng, L. Ungur, W. Wernsdorfer, F.-S. Guo, L. F. Chibotaru, M.-L. Tong, *Inorg. Chem.* **2012**, *51*, 8538-8544; d) Y. Rechkemmer, J. E. Fischer, R. Marx, M. Dörfel, P. Neugebauer, S. Horvath, M. Gysler, T. Brock-Nannestad, W. Frey, M. F. Reid, and J. van Slageren, *J. Am. Chem. Soc.* **2015**, *137*, 13114-13120; e) K. S. Pedersen, J. Dreiser, H. Weihe, R. Sibille, H. V. Johannesen, M. A. Sørensen, B. E. Nielsen, M. Sigris, H. Mutka, S. Rols, J. Bendix, and S. Piligkos, *Inorg. Chem.* **2015**, *54*, 7600-7606.
- [19] G. Novitchi, W. Wernsdorfer, L. F. Chibotaru, J.-P. Costes, C. E. Anson and A. K. Powell, *Angew. Chem. Int. Ed.* **2009**, *48*, 1614-1619.
- [20] T. Fukuda, N. Shigeyoshi, T. Yamamura and N. Ishikawa, *Inorg. Chem.* **2014**, *53*, 9080-9086.
- [21] a) H. L. C. Feltham, Y. Lan, F. Kloewer, L. Ungur, L. F. Chibotaru, A. K. Powell, S. Brooker *Chem. Eur. J.* **2011**, *17*, 4362-4365; b) M. E. Boulon, G. Cucinotta, J. Luzon, C. Degl'Innocenti, M. Perfetti, K. Bernot, G. Calvez, A. Caneschi, R. Sessoli, *Angew. Chem. Int. Ed.* **2013**, *52*, 350-354; c) L. Ungur, J. J. Le Roy, I. Korobkov, M. Murugesu and L. F. Chibotaru, *Angew. Chem., Int. Ed.*, **2014**, *53*, 4413 d) S. K. Singh, T. Gupta, M. Shanmugan, G. Rajaraman *Chem. Commun.* **2014**, *50*, 15513-15516; e) N. F. Chilton, C. A. P. Goodwin, D. P. Mills and R. E. P. Winpenny *Chem. Commun.*, **2015**, *51*, 101-103; f) E. Lucaccini, M. Briganti, M. Perfetti, L. Vendier, J.-P. Costes, F. Totti, R. Sessoli, L. Sorace *Chem. Eur. J.* **2016**, *22*, 5552-5562; g) J.-P. Costes, S. Titos-Padilla, I. Oyarzabal, T. Gupta, C. Duhayon, G. Rajaraman and E. Colacio, *Inorg. Chem.* **2016**, *55*, 4428-4440.
- [22] L. Li, S. Liu, H. Li, W. Shi and P. Cheng, *Chem. Commun.* **2015**, *51*, 10933-10936.
- [23] a) J. D. Rinehart and J. R. Long, *Dalton Trans.* **2012**, *41*, 13572-13574; b) K. R. Meihaus, J. D. Rinehart and J. R. Long, *Inorg. Chem.* **2011**, *50*, 8484-8489.
- [24] D. Casanova, M. Llunel, P. Alemany and S. Alvarez, *Chem. Eur. J.* **2005**, *11*, 1479-1494.
- [25] M. A. Aldamen, S. Cardona-Serra, J. M. Clemente-Juan, E. Coronado, A. Gaita-Ariño, C. Martí-Gastaldo, F. Luis and O. Montero, *Inorg. Chem.* **2009**, *48*, 3467-3479.
- [26] A. Abragam and B. Bleaney in *Electron Paramagnetic Resonance of Transition Ions*, Dover Publications, Inc. New York, **1986**.
- [27] a) A. Caneschi, A. Dei, D. Gatteschi, S. Poussereau and L. Sorace, *Dalton Trans.* **2004**, 1048-1055; b) V. Tangoulis and A. Figuerola, *Chem. Phys.* **2007**, *340*, 293-301; c) L. Sorace, C. Sangregorio, A. Figuerola, C. Benelli and D. Gatteschi, *Chem. Eur. J.* **2009**, *15*, 1377-1388; d) S. Ghosh, S. Datta, L. Friend, S. Cardona-Serra, A. Gaita-Ariño, E. Coronado and S. Hill, *Dalton Trans.* **2012**, *41*, 13697-13704; e) U. J. Williams, B. D. Mahoney, P. T. DeGregorio, P. J. Carroll, E. Nakamaru-Ogiso, J. M. Kikkawa, and E. J. Schelter, *Chem. Commun.* **2012**, *48*, 5593-5595; f) E. M. Pineda, N. F. Chilton, R. Marx, M. Dörfel, D. O. Sells, P. Neugebauer, S. Jiang, D. Collison, J. van Slageren, E. J. L. McInnes and R. E. P. Winpenny, *Nature Commun.* **2014**, *5*, 5243; g) J. van Slageren *Topics in Current Chemistry*, **2012**, *321*, 199-234; h) Y. Rechkemmer, J. E. Fischer, R. Marx, M. Dörfel, P. Neugebauer, S. Horvath, M. Gysler, T. Brock-Nannestad, W. Frey, M. F. Reid, J. van Slageren, *J. Am. Chem. Soc.*, **2015**, *137*, 13114-13120.
- [28] S. Stoll and A. Schweiger, *J. Magn. Reson.* **2006**, *178*(1), 42-55.
- [29] N. F. Chilton, R. P. Anderson, L. D. Turner, A. Soncini and K. S. Murray, *J. Comput. Chem.* **2013**, *34*, 1164-1175.
- [30] L. Sorace and D. Gatteschi in *Lanthanides and Actinides in Molecular Magnetism*, (Eds.: R. Layfield, M. Murugesu), Wiley-VCH, Weinheim **2015**, pp. 1-26.
- [31] Since PPMS used for high frequency measurements is less sensitive than the SQUID used for low frequency measurements, the high frequency ac data is noisier, as shown in the supplementary Figure S3.
- [32] P.-E. Car, M. Perfetti, M. Mannini, A. Favre, A. Caneschi, R. Sessoli *Chem. Commun.* **2011**, *47*, 3751-3753.
- [33] L. Vergnani, A. Barra, P. Neugebauer, M. J. Rodriguez-Douton, R. Sessoli, L. Sorace, W. Wernsdorfer and A. Cornia, *Chem. Eur. J.* **2012**, *18*, 3390-3398.
- [34] Y. Rechkemmer, F. D. Breitgoff, M. van der Meer, M. Atanasov, M. Haki, M. Orlita, P. Neugebauer, F. Neese, B. Sarkar and J. van Slageren, *Nature Comm.* **2016**, *7*, 10467.
- [35] K. N. Shrivastava, *Phys. Stat. Sol. (b)*, **1983**, *117*, 437-458
- [36] F. Pointillart, K. Bernot, S. Golhen, B. Le Guennic, T. Guizouarn, L. Ouahab, O. Cador, *Angew. Chem. Int. Ed.* **2015**, *54*, 1504-1507.
- [37] a) Q.-W. Xie, S.-Q. Wu, W.-B. Shi, C.-M. Liu, A.-L. Cui and H.-Z. Kou, *Dalton Trans.* **2014**, *43*, 11309-11316; b) J. Long, R. Vallat, R. A. S. Ferreira, L. D. Carlos, F. A. Almeida Paz, Y. Guari and J. Lariónova, *Chem. Commun.* **2012**, *48*, 9974-9976; c) M. A. Palacios, S. Titos-Padilla, J. Ruiz, J. M. Herrera, S. J. A. Pope, E. K. Brechin and E. Colacio, *Inorg. Chem.* **2014**, *53*, 1465-1474; d) J. Long, J. Rouquette, J. M. Thibaud, R. A. Ferreira, L. D. Carlos, B. Donnadieu, V. Vieru, L. F. Chibotaru, L. Konczewicz, J. Haines, Y. Guari and J. Lariónova, *Angew. Chem. Int. Ed.* **2015**, *54*, 2236-2240.
- [38] A. Watanabe, A. Yamashita, M. Nakano, T. Yamamura and T. Kajiwara, *Chem. Eur. J.* **2011**, *17*, 7428-7432.
- [39] N. F. Chilton, D. Collison, E. J. L. McInnes, R. E. P. Winpenny and A. Soncini, *Nat. Commun.* **2013**, *4*, 2551-2557.

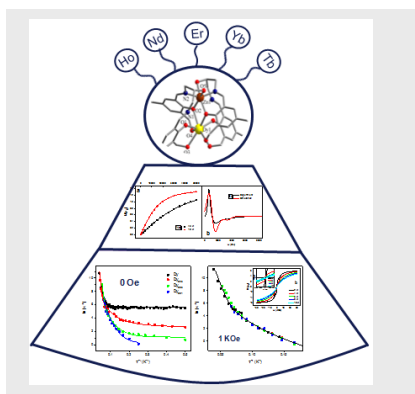
FULL PAPER

Entry for the Table of Contents (Please choose one layout)

Layout 1:

FULL PAPER

EPR spectroscopy and dc magnetic studies were used to probe the anisotropic magnetic properties of a series of ZnLn compounds, showing clear deviations from behaviour predicted on the basis of simple electrostatic model. The Dy^{III} derivative further showed a rich magnetization dynamics, for which multiple relaxation mechanisms were identified. Its activation barrier is one of the highest reported for dinuclear Zn-Dy systems.



Author(s), Corresponding Author(s)*

Page No. – Page No.

Title

Layout 2:

FULL PAPER

((Insert TOC Graphic here; max. width: 11.5 cm; max. height: 2.5 cm))

Author(s), Corresponding Author(s)*

Page No. – Page No.

Title

Text for Table of Contents